

SUPPLEMENTARY MATERIAL

CHARACTERIZATION OF THE DIFFERENT NANOPARTICLES:

Concentration of the different suspensions:

To estimate iron concentrations in the different suspensions containing magnetosome minerals (coated or uncoated) or IONPs, both types of nanoparticles were mixed with hydrochloric acid and hydrogen peroxide to produce Fe³⁺ ions complexed with potassium thiocyanate, whose quantity was determined by absorbance at 476 nm.

TEM characterization:

For transmission electron microscopy (TEM) analyses, 5 µl of each nanoparticle suspension at a concentration of 200 µg of iron per mL was washed twice with distilled water and deposited on top of a carbon-coated copper grid (oxford instruments) and dried. Images were recorded using a JEOL LaB6 JEM-2100 at 200 KeV.

Dynamic light scattering measurements:

The surface charges of 1 mg of the different nanoparticles mixed in water were estimated from dynamic light scattering measurements using a Nano-ZS (Red Badge) ZEN 3600 device (Malvern Instruments, Malvern, UK). The zeta potential of the different nanoparticles was measured as a function of pH over the pH range from 2 to 11 by adjusting the suspensions' pH with NaOH or HCl solutions at 25°C.

Stability of the different suspensions:

The colloidal stability of the different nanoparticle suspensions was also evaluated by optical density measurements on a UviLine9400 Secomam spectrophotometer. 1 mg per mL of water of each suspension was transferred into a quartz vessel, after rapid homogenization, and the variation of the absorption with time was measured at 476 nm during 20 minutes.

Fourier transform infrared (FT-IR) measurements:

To identify the various chemical groups at the nanoparticle surface, Fourier transform infrared (FTIR) spectra of powders containing lyophilized uncoated and coated magnetosome minerals as well as IONPs were recorded between 4000 and 400 cm^{-1} with a resolution of 4 cm^{-1} using a Bucker Vertex 70.

Elemental analysis (CHNS):

CHNS measurements were carried out using an Elemental Flash EA 1112 analyzer manufactured by Thermo Fischer Scientific on the lyophilized nanoparticule suspensions containing each 10 mg of iron in order to determine the suspensions' percentages of carbon, nitrogen, hydrogen and sulfur.

Magnetic measurements:

For magnetic measurements, suspensions containing ~10 mg of iron of each nanoparticle (IONPs, uncoated and coated magnetosomes) were lyophilised, introduced in nonmagnetic polypropylene capsules and stored in anaerobic jars. Room temperature magnetic measurements were carried out using a vibrating sample magnetometer (VSM Model 3900 manufactured by Princeton Measurements Co.). Hysteresis loops were acquired in a maximum 1 T field from which saturation magnetization, M_s following a high field slope correction and coercivity, $\mu_0 H_c$, were derived. Low temperature magnetic behaviour was measured on a Magnetic Properties Measurement System (MPMS XL-5 EverCool) manufactured by Quantum Design. Isothermal remanent magnetization (IRM) induced in a 2.5 T magnetic field was acquired at 10 K ($^{2.5T} \text{IRM}_{10K}$) and monitored on warming to 300 K in a zero (< 500 nT) magnetic field. Prior to $^{2.5T} \text{IRM}_{10K}$ acquisition, suspensions underwent two pre-treatments. The zero-field cooling (ZFC) pre-treatment consists of cooling the suspensions from 300 K to 10 K in a zero magnetic field before $^{2.5T} \text{IRM}_{10K}$ acquisition. The

field cooling (FC) pre-treatment consists of cooling the suspensions from 300 K to 10 K in a 2.5 T magnetic field prior to $^{2.5T}IRM_{10K}$ acquisition. The mineral speciation of the magnetosomes and any alteration of magnetite towards maghemite may be assessed by observing the behaviour of the Verwey transition, in the ZFC-FC data.

Pyrogenicity estimate with the LAL Assay:

Limulus amoebocyte lysate (LAL) tests were carried out under sterile conditions using the 88282 ThermoScientific kit "*Pierce LAL Chromogenic Endotoxin Quantitation Kit*". 1 ml of each suspension was homogenized by sonication, washed with pyrogen-free water and heated at 70 °C during 10 minutes to denature any residual proteins that could interfere with the LAL assay. 25 µL of each suspension containing 10 µg of iron were then introduced in a 96-well and maintained at 37 °C throughout the duration of the experiment. 25 µl of the LAL kit solution were added to initiate the reaction. After 10 minutes of reaction, 50 µl of the chromogenic substrate were added to the well. After 6 minutes, 25 µl of acetic acid were added to stop the reaction and the optical density of the obtained suspensions was measured at 405 nm using a microplate reader. The endotoxin concentration was then estimated using the calibrating curve provided with the kit. To verify that the LAL test does not interfere with the nanoparticles, a recovery rate, defined as $C_{total}/C1+C2$ was measured, where C_{total} is the endotoxin concentration of the nanoparticle suspensions mixed with a known amount of endotoxin of 0.5 UE/mL, C1 is the concentration of endotoxins in the different suspensions of nanoparticles and $C2 = 0.5$ UE/mL.

Pyrogenicity estimate with the rabbit test (ISO 10993-11):

A rabbit test was also carried out according to ISO10993-11 by using a suspension containing 5 mg/mL of M-PLL, which was first placed in an ultrasonic bath for 2 minutes for homogenization. 1 ml of this suspension was then diluted in 119 ml of 0.9% NaCl. The

temperature of the suspension was maintained at 37 °C for 30 minutes, after which the suspension was homogenized and administered intravenously to one rabbit at a dose of 10 ml/kg. The body temperature of the rabbit was measured every 30 minutes during 3 hours.

Cytotoxicity of the PLL, M-PLL and IONPs towards healthy 3T3 cells according to ISO 10993-5:

Cytotoxicity of uncoated magnetosomes, poly-L-lysine alone (PLL), M-PLL and IONPs was tested on and 3T3 (mouse fibroblast) cell lines using an MTT assay. This technique measures the ability of mitochondrial enzymes to reduce 3-(4,5-dimethylthiazol-2-yl)-2,5-diphenyltetrazolium bromide to purple formazan crystals. 3T3 cells bought from ATCC (USA) were seeded at a density of $5 \cdot 10^3$ cells per well in a 96-well plate and allowed to adhere overnight. Subsequently, the Dulbecco's Modification of Eagle's Medium (DMEM) without L-glutamine, supplemented with 10 % Newborn calf serum (NBCS), was removed and replaced by 100 μ L of culture medium containing different nanoparticle concentrations (1000, 500, 125, 62.5, 31.25 or 15.62 μ g/mL). Cells were incubated at 37 °C in a 5% CO₂ humidified atmosphere for 24 hours. Following incubation, cells were washed with a PBS solution and incubated with 100 μ L of MTT (1 mg/mL) for an additional 2 hours at 37°C. The insoluble product was then dissolved by the addition of 100 μ L of an isopropanol solution. The PBS washed cells represent the blank control. The optical density (OD) of the solubilized formazan, which reflects the relative viable cell number, was measured at 540 nm using a microplate reader. Percentage of cellular inhibition (% inhibition) was estimated using the formula, % inhibition = $[1 - (OD_{TC}/OD_{UC})] \times 100$, where OD_{TC} and OD_{UC} correspond to the optical density, measured at 540 nm, of cells with nanoparticles and of cells without nanoparticles, respectively. The experiments were carried out in biological triplicates. Dose response curves were obtained for all suspensions, enabling the determination of half inhibitory concentrations, IC₅₀.

Figure S5a shows that the percentage of cell inhibition is lower than 30%. This indicates that M-PLL is biocompatible according to the criteria of ISO 10993-5. M-PLL cytotoxicity towards tumour glioblastoma cells was studied by bringing into contact GL-261 cells with various concentrations of M-PLL for 24 hours. Supplementary Fig. 3(b) shows that percentage of cell inhibition is strongly enhanced in the presence of tumor cells compared with normal 3T3 fibroblast cell, resulting in measurable half maximum inhibitory concentrations, IC_{50} , of 270 $\mu\text{g/mL}$. M-PLL cytotoxicity towards GL-261 cells, which is larger than that measured for uncoated magnetosome minerals, could be due to relatively significant PLL cytotoxicity, (i), (Figure S5b). Higher cytotoxicity towards tumour than normal cells is desirable since it potentially strengthens treatment safety and efficacy. Although it is significant, M-PLL intrinsic cytotoxicity is much less than that of standard cytotoxic cancer drugs such as doxorubicin and temozolomide, (ii), suggesting that its main mode of action is not pharmaceutical.

Cytotoxicity of the PLL, M-PLL and IONPs suspensions towards tumor GL-261 cells:

Cytotoxicity of uncoated magnetosomes, poly-L-lysine alone (PLL), M-PLL and IONPs was also tested on and GL-261 tumor cell lines using an MTT assay, following the same protocol as that described above for 3T3 cells, except that the culture medium was RPMI 1640 supplemented with 10 % foetal bovine serum (FBS) for GL261 cells.

Acute systemic toxicity:

Acute systemic toxicity was estimated according to ISO standard 10993-11. C57/BL6 mice received intravenously through its tail 100 μl of a suspension containing 2 or 4 mg of M-PLL (condition 1), 100 μl of a suspension containing 2 or 4 mg of IONPs (condition 2) or 100 μl of glucose 5 % (condition 3). For each of these three conditions, five mice were used. Over a

10-day period following injection, potential acute toxicity was evaluated by monitoring mouse body weight loss as well as unusual mouse behavior.

MR imaging:

MR imaging and treatment were performed with a 7T small animal MRI scanner (Bruker Biospin, Ettlingen, Germany). Animals were anesthetized with isoflurane (2 %) and placed into the MRI scanner. The body temperature and the respiratory rate were monitored during the whole procedure. For the tumor growth follow up, T2 weighted (echo time TE $\frac{1}{4}$ 12 ms, repetition time TR $\frac{1}{4}$ 4200 ms, acquisition time 202 s for each orientation) and contrast enhanced T1-weighted (TE $\frac{1}{4}$ 8 ms, TR $\frac{1}{4}$ 2500 ms, acquisition time 300 s for each orientation) MR images were acquired in three orientations and used to localise the tumour in the brain, and to measure its dimensions. For both contrasts, a rapid acquisition with refocused echoes (RARE) sequence was used with the following parameters: 32_32mm field of view (matrix size 256_256, zero-fill phase acceleration factor of 1.34, RARE factor 8), sufficient number of slices to cover the whole brain in each orientation (slice thickness 1 mm).

SUPPLEMENTARY TABLES:

Table S1: Heating characteristics of mice belonging to groups 1, 3 and 5 during the various magnetic sessions.

Table S2: Treatment protocols for each mouse belonging to groups 1 to 6

Table S3: Physical and chemical properties of magnetosomes minerals, M-PLL and IONPs.

Table S4: Median survival day and associated p-value for mice belonging to groups 1 to 6.

SUPPLEMENTARY FIGURES:

Figure S1: Variation as a function of time of the absorbance, measured at 480, of suspensions containing 1mg/mL in iron of uncoated magnetosome minerals (Magnetosome Minerals), M-PLL and IONPs

Figure S2: Histogram size distribution, obtained from TEM images, of magnetosomes (n=400) inside MSR-1 strain, (a), and for magnetosome (n=400) minerals, (b). Magnetosome minerals have an average size of 40.5 ± 8.5 nm, which is identical to size distributions analysed from intact MSR-1 bacteria. Thus, the purification process does not modify magnetosome particle size.

Figure S3: (a), Hysteresis curves of magnetosome minerals, M-PLL and IONPs. (b), Low temperature remanence demagnetization curves (Zero field cooled, ZFC, and field cooled, FC) of whole MSR-1 magnetotactic bacteria showing the Verwey transition. (c), Low temperature remanence demagnetization curves (Zero field cooled, ZFC, and field cooled, FC) of uncoated magnetosome minerals showing the absence of the Verwey transition.

Figure S4: (a), FTIR spectra of magnetosome minerals, M-PLL, and IONPs. (b), Variations of Zeta potentials as a function of pH for magnetosome minerals (Mg. minerals), M-PLL, and IONPs. (c), Weight percentages of carbon and nitrogen in IONPs, magnetosome minerals (Mg. minerals) and M-PLL.

Figure S5: Percentage of cell inhibition of 3T3 cells, (a), and GL-261 cells, (b), brought into contact with various concentrations (1000, 500, 125, 62.5, 31.25 or 15.62 $\mu\text{g/mL}$) of PLL, magnetosome minerals (Mg. minerals), M-PLL and IONPs.

Figure S6: Mouse body weight variation following injection in the tail of mice of 2 or 4 mg of M-PLL, 2 or 4 mg of IONPs, or 5% glucose, measured during 10 days following injection.

Figure S7: T2 weighted MR images of tumor in rat brain (tumor circle in red) before magnetosome injection, 10 or 13 days following tumor cell implantation (D10 and D13), and at D16, 3 days following injection of 20 μ l of a suspension containing magnetosomes at a concentration of 20 mg/mL in a RG2 tumor of size 20 mm³.

Figure S8: N: Necrotic area. (a), Representative H&E section of subcutaneous GL-261 tumor injected with 25 μ g of iron per mm³ of tumor in M-PLL followed by one MS (M-PLL (6 H) + AMF). (b), enlargement of (a). Tumor was collected 6 hours after the injection. (c), Representative H&E section of subcutaneous GL-261 tumor injected with 25 μ g of iron per mm³ of tumor in M-PLL (M-PLL (6 H) – AMF). (d), enlargement of (c). Tumor was collected 6 hours after the injection. (e), Representative H&E section of subcutaneous GL-261 tumor injected with 25 μ g of iron per mm³ of tumor in M-PLL followed by two MS (M-PLL (72 H) + AMF). (f), enlargement of (e). Tumor was collected 72 hours after the injection. (g), Representative H&E sections of subcutaneous GL-261 tumor injected with 25 μ g of iron per mm³ of tumor in M-PLL (M-PLL (72 H) – AMF). (h), enlargement of (g). Tumor was collected 72 hours after the injection.

Figure S9: (a), Representative Perls prussian blue section of subcutaneous GL-261 tumor injected with 25 μ g of iron per mm³ of tumor in M-PLL followed by one MS (M-PLL (6 H) + AMF). (b), enlargement of (a). Tumor was collected 6 hours after the injection. (c), Representative Perls prussian blue section of subcutaneous GL-261 tumor injected with 25 μ g of iron per mm³ of tumor in M-PLL (M-PLL (6H) – AMF). (d), enlargement of (c). Tumor was collected 6 hours after the injection. (e), Representative Perls prussian blue section of subcutaneous GL-261 tumor injected with 25 μ g of iron per mm³ of tumor in M-PLL followed by two MS (M-PLL (72 H) + AMF). (f), enlargement of (e). Tumor was collected 72 hours after the injection. (g), Representative Perls prussian blue sections of subcutaneous

GL-261 tumor injected with 25 μg of iron per mm^3 of tumor in M-PLL (M-PLL (72 H) – AMF). (h), enlargement of (g). Tumor was collected 72 hours after the injection.

Figure S10: N: Necrotic area. (a), Representative H&E section of subcutaneous GL-261 tumor injected with 25 μg of iron per mm^3 of tumor in IONPs followed by one MS (IONPs (6H) + AMF). (b), enlargement of (a). Tumor was collected 6 hours after the injection. (c), Representative H&E section of subcutaneous GL-261 tumor injected with 25 μg of iron per mm^3 of tumor in IONPs (IONPs (6 H) – AMF). (d), enlargement of (c). Tumor was collected 6 hours after the injection. (e), Representative H&E section of subcutaneous GL-261 tumor injected with 25 μg of iron per mm^3 of tumor in IONPs followed by two MS (IONPs (72 H) + AMF). (f), enlargement of (e). Tumor was collected 72 hours after the injection. (g), Representative H&E sections of subcutaneous GL-261 tumor injected with 25 μg of iron per mm^3 of tumor in IONPs (IONPs (72 H) – AMF). (h), enlargement of (g). Tumor was collected 72 hours after the injection.

Figure S11: (a), Representative Perls prussian blue section of subcutaneous GL-261 tumor injected with 25 μg of iron per mm^3 of tumor in IONPs followed by one MS (IONPs (6H) + AMF). (b), enlargement of (a). Tumor was collected 6 hours after the injection. (c), Representative Perls prussian blue section of subcutaneous GL-261 tumor injected with 25 μg of iron per mm^3 of tumor in IONPs (IONPs (6 H) – AMF). (d), enlargement of (c). Tumor was collected 6 hours after the injection. (e), Representative Perls prussian blue section of subcutaneous GL-261 tumor injected with 25 μg of iron per mm^3 of tumor in IONPs followed by two MS (IONPs (72 H) + AMF). (f), enlargement of (e). Tumor was collected 72 hours after the injection. (g), Representative Perls prussian blue sections of subcutaneous GL-261 tumor injected with 25 μg of iron per mm^3 of tumor in IONPs (IONPs (72 H) – AMF). (h), enlargement of (g). Tumor was collected 72 hours after the injection.

Figure S12: N: Necrotic area. (a), H&E section of subcutaneous GL-261 tumor injected with 50 μ l of a 5 % glucose suspension followed by one MS (Glu. (6H) + AMF). (b), enlargement of (a). Tumor was collected 6 hours after injection. (c), H&E section of subcutaneous GL-261 tumor injected with 50 μ l of a 5 % glucose suspension (Glu. (6H) – AMF). (d), enlargement of (c). Tumor was collected 6 hours after injection. (e), H&E section of subcutaneous GL-261 tumor injected with 50 μ l of a 5 % glucose suspension followed by two MS (Glu. (72H) + AMF). (f), enlargement of (e). Tumor was collected 72 hours after the injection. (g), H&E section of subcutaneous GL-261 tumor injected with 50 μ l of a 5 % glucose suspension (Glu. (72 H) – AMF). (h), enlargement of (g). Tumor was collected 72 hours after injection.

Figure S13: (a), Representative Perls Prussia blue section of subcutaneous GL-261 tumor injected with 50 μ l of a 5 % glucose suspension followed by one MS (Glu. (6 H) + AMF). (b), enlargement of (a). Tumor was collected 6 hours after the injection. (c), Representative Perls prussian blue section of subcutaneous GL-261 tumor injected with 50 μ l of a 5 % glucose suspension (Glu. (6H) _AMF). (d), enlargement of (c). Tumor was collected 6 hours after the injection. (e), Representative Perls prussian blue section of subcutaneous GL-261 tumor injected with 50 μ l of a 5 % glucose suspension followed by two MS (Glu. (72 H) + AMF). (f), enlargement of (e). Tumor was collected 72 hours after the injection. (g), Representative Perls prussian blue section of subcutaneous GL-261 tumor injected with 50 μ l of a 5 % glucose suspension (Glu. (72 H) – AMF). (h), enlargement of (g). Tumor was collected 72 hours after the injection.

Treatment M-PLL (group 1)				
Days of AMF application	Number of mice with intratumoral heating at 43-46°C	SAR (W/g _{Fe})	T _{max} °C	Number of reinjected mice
D0	10	40.2	45.8 ± 1.5	0
D2	9		44.9 ± 0.72	0
D4	6		45.2 ± 0.76	0
D7	3		46.1 ± 1.18	0
D9	1		45.2	0
D11	1		45.7	1
D14	2		50.6 ± 7.9	1
D16	3		45.7 ± 0.85	1
D18	4		45.1 ± 0.46	1
D21	4		44.7 ± 0.96	0
D23, D25, D28, D30, D32				0
Treatment IONPs (group 3)				
Days of AMF application	Number of mice with intratumoral heating at 43-46°C	SAR (W/g _{Fe})	T _{max} °C	Number of reinjected mice
D0	10	25.9	44.3 ± 0.56	0
D2	3		45.1 ± 1.39	0
D4	5		45.2 ± 2.1	4
D7	6		45.3 ± 0.84	1
D9	6		45.9 ± 1.7	1
D11	4		44.4 ± 2.7	0
D14	2		47.1 ± 7.2	0
D16	1		46.5	0
D18	1		44.2	0
D21, D23, D25, D28, D30, D32				0
Treatment glucose 5 % (group 5)				
Days of AMF application	Number of mice with intratumoral heating at 43-46°C	SAR (W/g _{Fe})	T _{max} °C	Number of reinjected mice
D0, D2, D4, D7, D9, D11, D14, D16, D18, D21, D23	0	0		0

Table S1

Groups number	Mice number	Injection	AMF	Days of injection	Days of AMF application and mean field intensity (mT)	Day of euthanasia
1	1	MPLL	yes	D0	D0 (21); D2-D4-D7-D9-D11-D14-D16-D18-D21 (27)	D250
	2	MPLL	yes	D0	D0 (19); D2 (24); D4 (22-24); D7-D9-D11-D14-D16-D18-D21-D23-D25 (27)	D250
	3	MPLL	yes	D0, D14	D0 (16-17); D2 (15-16); D4 (16-17); D7 (17); D9 (23-26); D11 (27); D14 (11); D16 (16); D18 (16-20); -D21 (19-22); D23 (22-27)	D25
	4	MPLL	yes	D0, D18	D0-D2-D4-D7-D9-D11-D14-D16 (27); D18 (23-27); D21 (16-20); D23 (14-23); D25 (22-23); D28 (22)	D30
	5	MPLL	yes	D0	D0 (19); D2 (20-21); D4-D7-D9-D11-D14-D16-D18-D21-D23-D25-D28-D30-D32 (27)	D250
	6	MPLL	yes	D0	D0 (16); D2 (20-21); D4-D7-D9-D11-D14-D16-D18-D21-D23-D25 (27)	D28
	7	MPLL	yes	D0, D16	D0 (22-24); D2 (23-24); D4 (26-27); D7-D9-D11-D14 (27); D16 (15-21); D18 (16-18); D21 (16-22); D23 (19-22)	D25
	8	MPLL	yes	D0	D0 (15); D2 (16); D4 (20-26); D7-D9-D11-D14-D16-D18-D21-D23-D25-D28-D30 (27)	D250
	9	MPLL	yes	D0	D0 (13); D2 (12-13); D4 (13-14); D7 (11-12); D9-D11-D14-D16-D18-D21-D23-D25-D28-D30-D32 (27)	D250
	10	MPLL	yes	D0, D11	D0 (23-24); D2 (24-25); D4 (19-21); D7 (17-19); D9 (25-26); D11 (16-17); D14 (20); D16 (20); D18 (20-22); D21 (21-22); D23-D25-D28-D30-D32 (27)	D44
2	11	MPLL	no	D0	/	D11
	12	MPLL	no	D0	/	D9
	13	MPLL	no	D0	/	D14
	14	MPLL	no	D0	/	D16
	15	MPLL	no	D0	/	D9
	16	MPLL	no	D0	/	D16
	17	MPLL	no	D0	/	D16
	18	MPLL	no	D0	/	D14
	19	MPLL	no	D0	/	D9
	20	MPLL	no	D0	/	D14
3	21	IONPs	yes	D0, D7	D0 (30-31); D2-D4-D7-D9-D11-D14 (27)	D14
	22	IONPs	yes	D0, D4	D0 (27-29); D2 (27); D4 (24-25); D7 (24-26); D9 (27); D11 (26)	D14
	23	IONPs	yes	D0, D4	D0 (26-27); D2 (27); D4 (18-22); D7 (26-27); D9 (23-26); D11 (23-25); D14 (24-25); D16 (27)	D18
	24	IONPs	yes	D0, D4	D0 (30); D2-D4 (27); D7 (25-26); D9 (26-27); D11-D14-D16-D18-D21-D23-D25-D28-D30 (27)	D32
	25	IONPs	yes	D0, D4	D0 (22-26); D2 (27); D4 (22-24); D7 (24-25); D9 (22-23); D9 (27); D11 (22-27)	D16
	26	IONPs	yes	D0	D0 (30); D2-D4-D7-D9-D11-D14-D16-D18-D21-D23-D25 (27)	D28
	27	IONPs	yes	D0	D0 (25-26); D2-D4-D7-D9-D11-D14-D16-D18-D21-D23-D25-D28-D30-D32 (27)	D44
	28	IONPs	yes	D0	D0 (27-28); D2-D4-D7-D9-D11-D14-D16-D18-D21 (27)	D250
	29	IONPs	yes	D0	D0 (22-24); D2 (25); D4 (26); D7 (25-26); D9 (25-26); D11 (26-27); D14-D16-D18 (27)	D21
	30	IONPs	yes	D0, D9	D0 (26-27); D2-D4-D7 (27); D9 (22-25); D11-D14-D16-D18-D21-D23-D25-D28 (27)	D250
4	31	IONPs	no	D0	/	D9
	32	IONPs	no	D0	/	D9
	33	IONPs	no	D0	/	D16
	34	IONPs	no	D0	/	D11
	35	IONPs	no	D0	/	D9
	36	IONPs	no	D0	/	D11
	37	IONPs	no	D0	/	D11
	38	IONPs	no	D0	/	D7
	39	IONPs	no	D0	/	D18
	40	IONPs	no	D0	/	D7
5	41	Glucose (5%)	yes	D0	D0-D2-D4-D7-D9-D11-D14 (27)	D16
	42	Glucose (5%)	yes	D0	D0-D2-D4-D7 (27)	D9
	43	Glucose (5%)	yes	D0	D0-D2-D4-D7-D9-D11-D14 (27)	D16
	44	Glucose (5%)	yes	D0	D0-D2-D4-D7 (27)	D9
	45	Glucose (5%)	yes	D0	D0-D2-D4-D7-D9 (27)	D11
	46	Glucose (5%)	yes	D0	D0-D2-D4-D7-D9-D11-D14-D16-D18 (27)	D21
	47	Glucose (5%)	yes	D0	D0-D2-D4-D7-D9-D11-D14-D16-D18-D21 (27)	D23
	48	Glucose (5%)	yes	D0	D0-D2-D4-D7-D9-D11-D14 (27)	D16
	49	Glucose (5%)	yes	D0	D0-D2-D4 (27)	D7
	50	Glucose (5%)	yes	D0	D0-D2-D4-D7-D9-D11 (27)	D14
6	51	Glucose (5%)	no	D0	/	D16
	52	Glucose (5%)	no	D0	/	D9
	53	Glucose (5%)	no	D0	/	D11
	54	Glucose (5%)	no	D0	/	D14
	55	Glucose (5%)	no	D0	/	D9
	56	Glucose (5%)	no	D0	/	D9
	57	Glucose (5%)	no	D0	/	D7
	58	Glucose (5%)	no	D0	/	D7
	59	Glucose (5%)	no	D0	/	D11
	60	Glucose (5%)	no	D0	/	D11

Table S2

Physical and Chemical Properties	Magnetosome minerals	M-PLL	IONPs
Size (nm)	40.5 ± 8.5	40.5 ± 8.5	20 ± 5; 17 ± 4
Thickness of coating (nm)		4-17	No visible
Endotoxins level (EU/mL/mg)	10-100	80	<50
Acute systemic toxicity (mg)		2 mg none	2 mg none
Zêta potential (mV) as function of pH	pH 2	pH 2	pH 2
	pH 4	pH 4	pH 4
	pH 6	pH 6	pH 6
	pH 8	pH 8	pH 8
	pH 10	pH 10	pH 10
	pH 12	pH 12	pH 12
	+18	+43	+7
	-8	+35	+6
	-1.5	+24.5	+7
	-27	+5	+5.5
	-35	-14	-2.2
	-45	-34	-20
FTIR (cm ⁻¹) peaks	Fe-O (610)	Fe-O (610)	Fe-O (610)
	Iron oxyde	Iron oxide	Iron oxide
	P-O (1000) C-H (3300) N-H (3400)	P-O (1000) C-H (2900) OH (3300) N-H (3400)	C-O (1050) C-O-C (1100) C-H (2850) O-H (3300)
	Organic residues	Organic residues	Starch polymer
	Organic residues	Poly-L-lysine	
CHNS (W) percentage in weight	C	C	C
	H	H	H
	N	N	N
	S	S	S
	0.53±0.01	0.92±0	1.43±0.01
	0.16±0	0.03±0	0
	0.03±0	0.04±0.01	0
Mineralogy	Maghemite (no verwey transition)	Maghemite (no verwey transition)	Maghemite
	M _s (Am ² /Kg)	M _s (Am ² /Kg)	M _s (Am ² /Kg)
Hysteretic parameters	64	70	47
	10	6	11
	H _c (mT)	H _c (mT)	H _c (mT)
	10	6	11

Table S3

	Treatment	Median Survival day	p-value
Group 1	M-PLL + AMF	147	< 0.0001
Group 2	M-PLL-AMF	14	0,2
Group 3	IONPs + AMF	24,5	< 0.0001
Group 4	IONPs -AMF	10	0.629
Group 5	Glucose 5 % + AMF	15	0.05
Group 6	Glucose 5 % -AMF	10	

Table S4

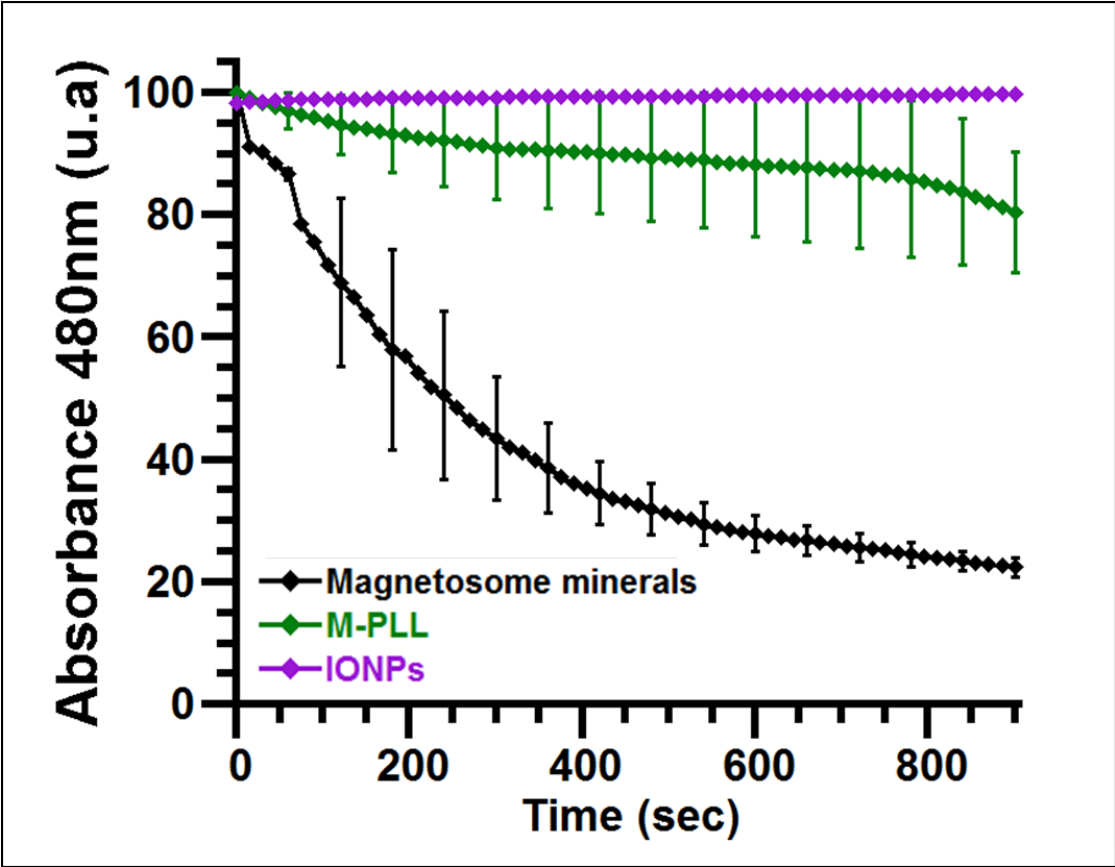


Figure S1

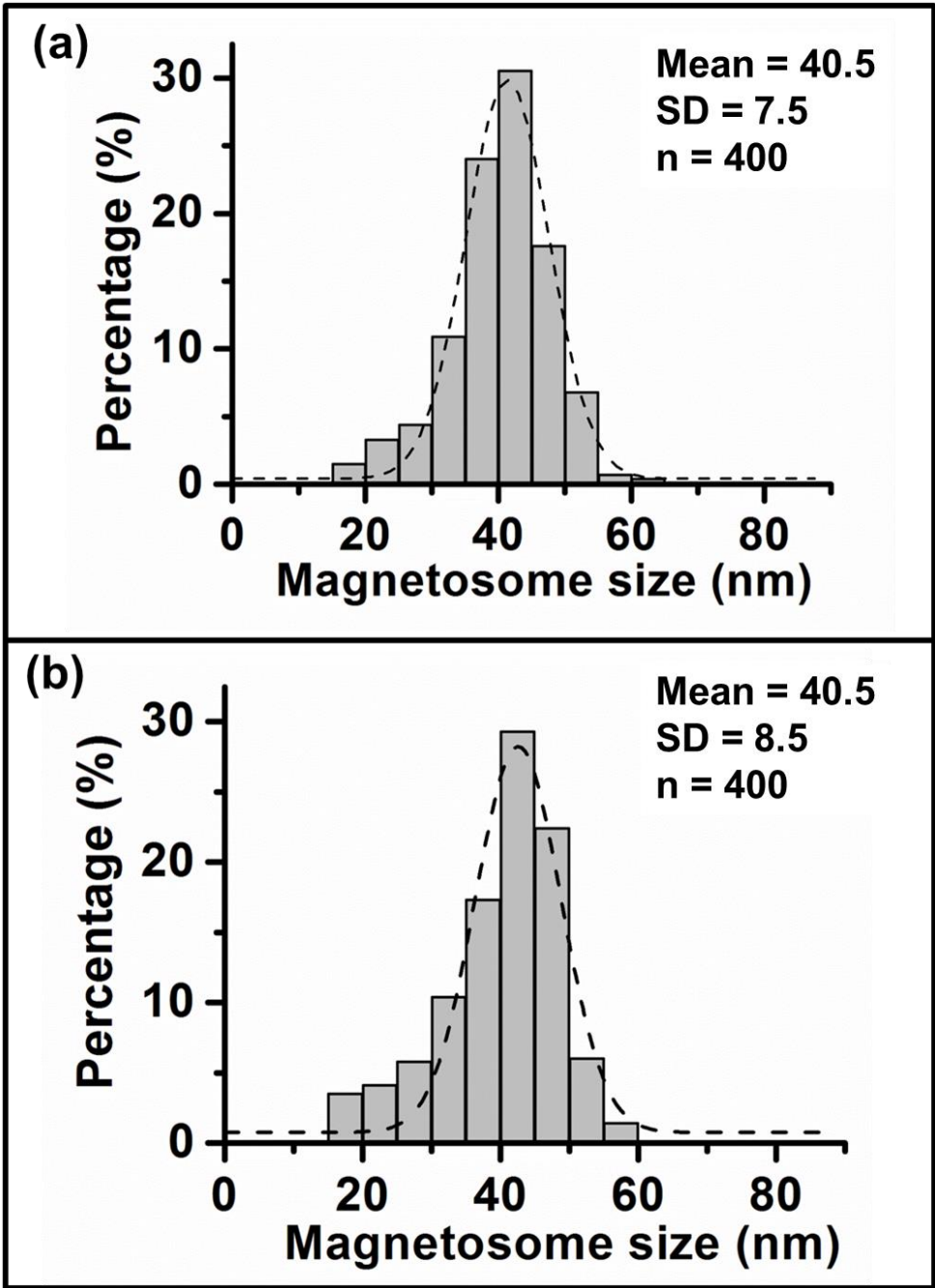


Figure S2

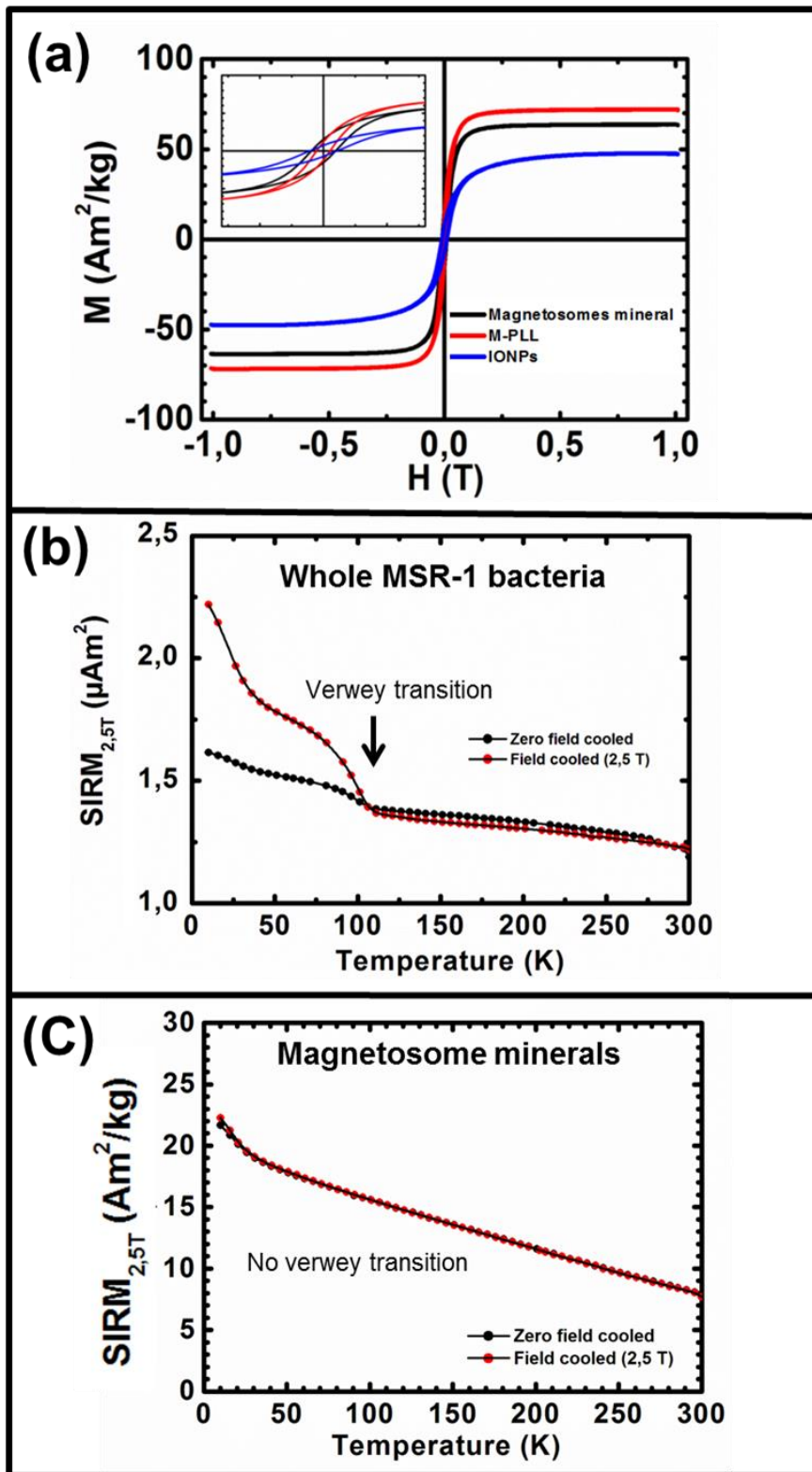


Figure S3

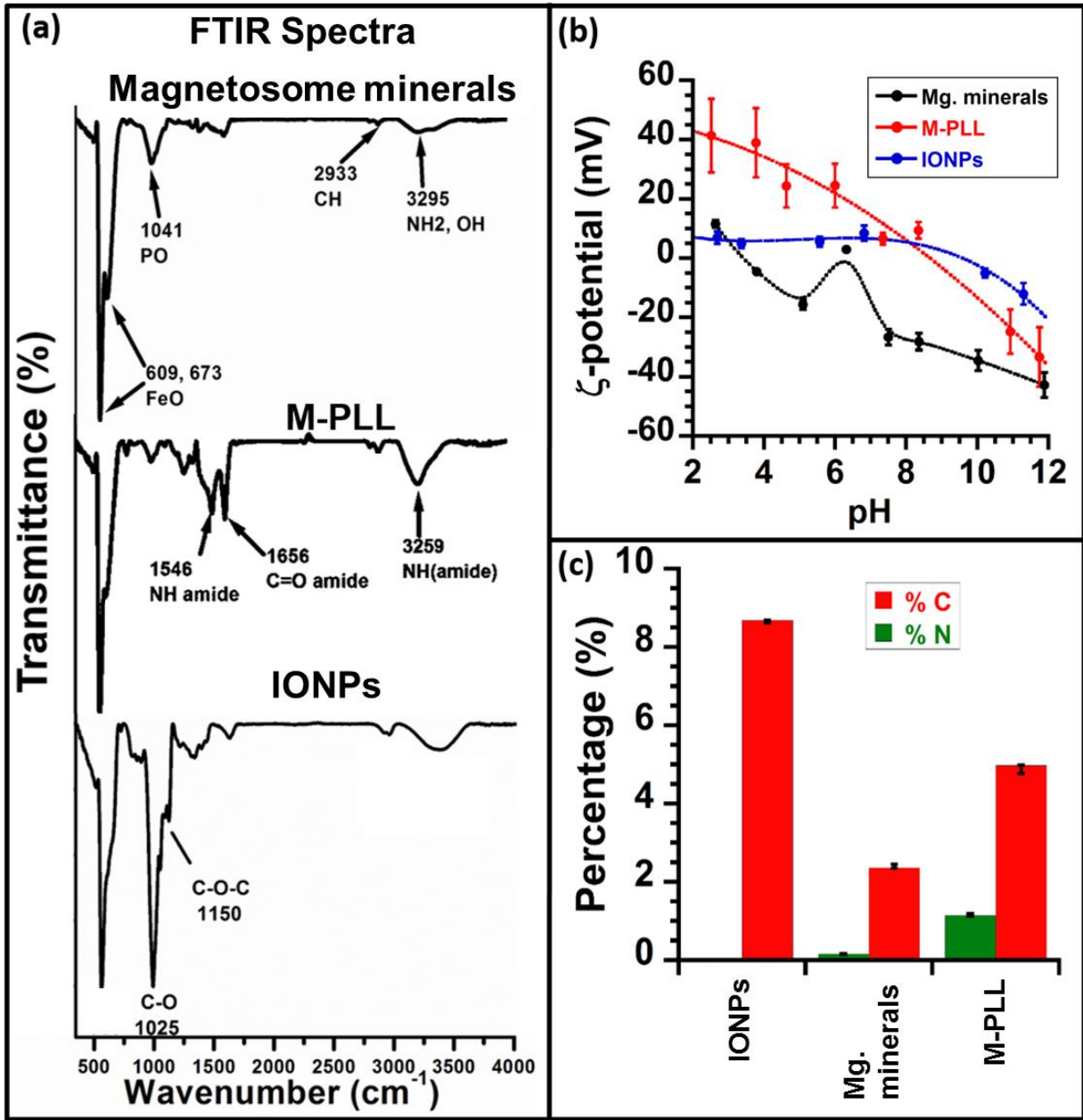


Figure S4

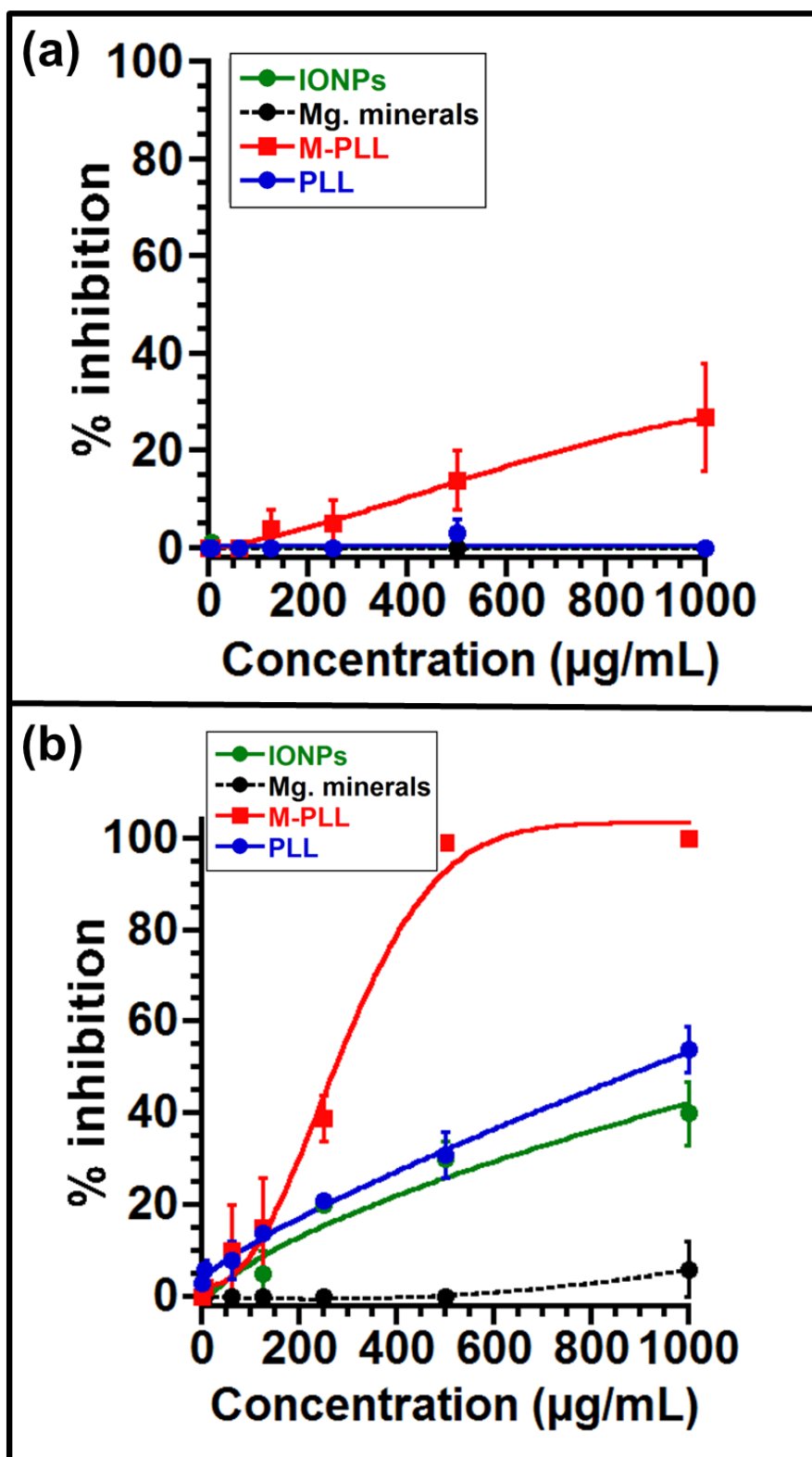


Figure S5

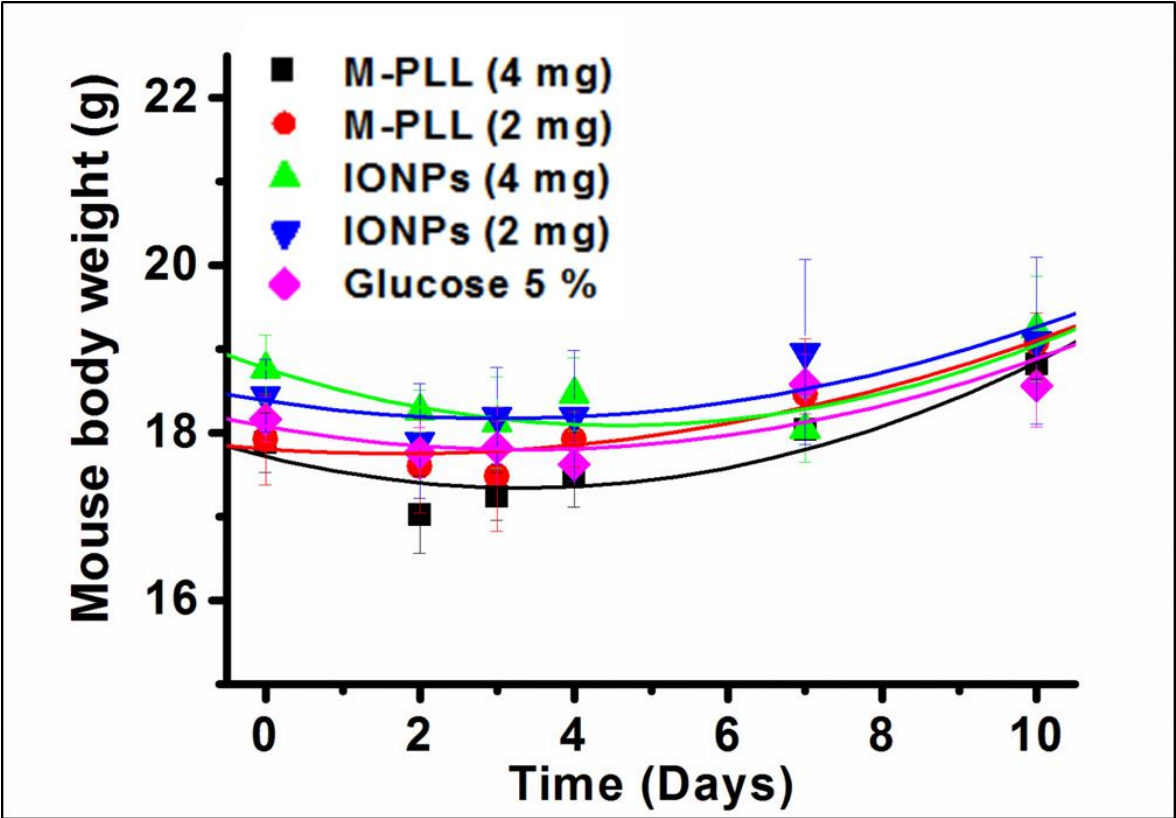
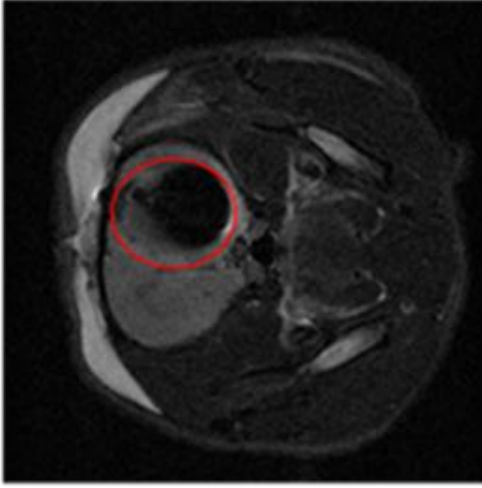
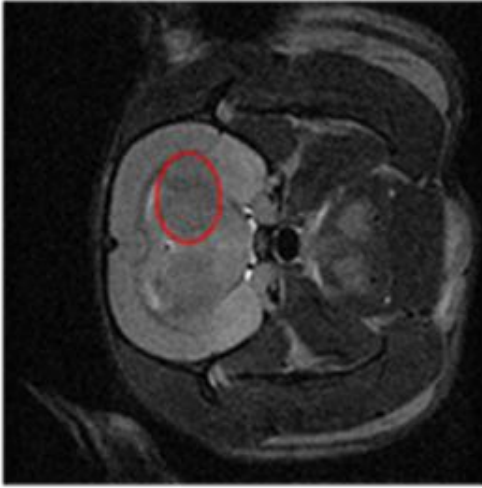


Figure S6

D16



D13



D10

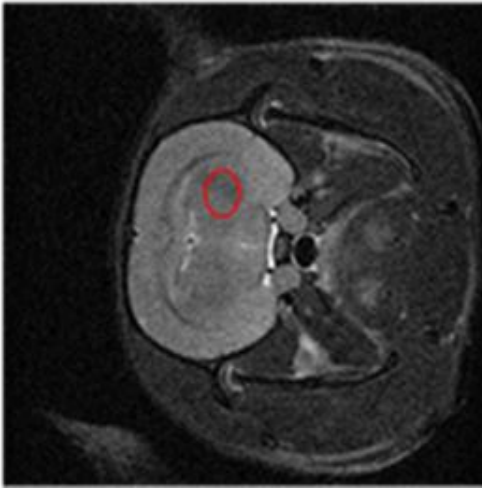


Figure S7

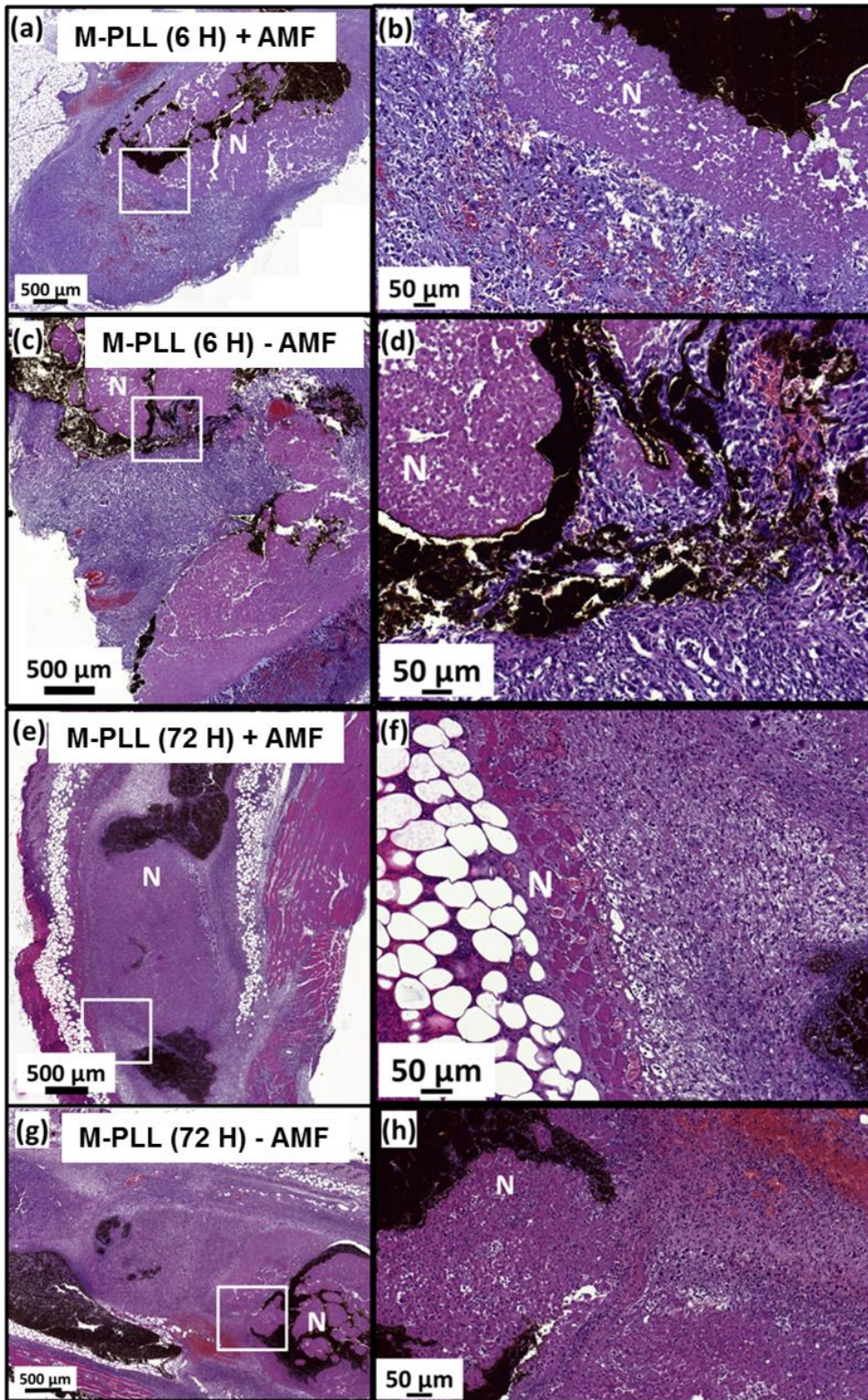


Figure S8

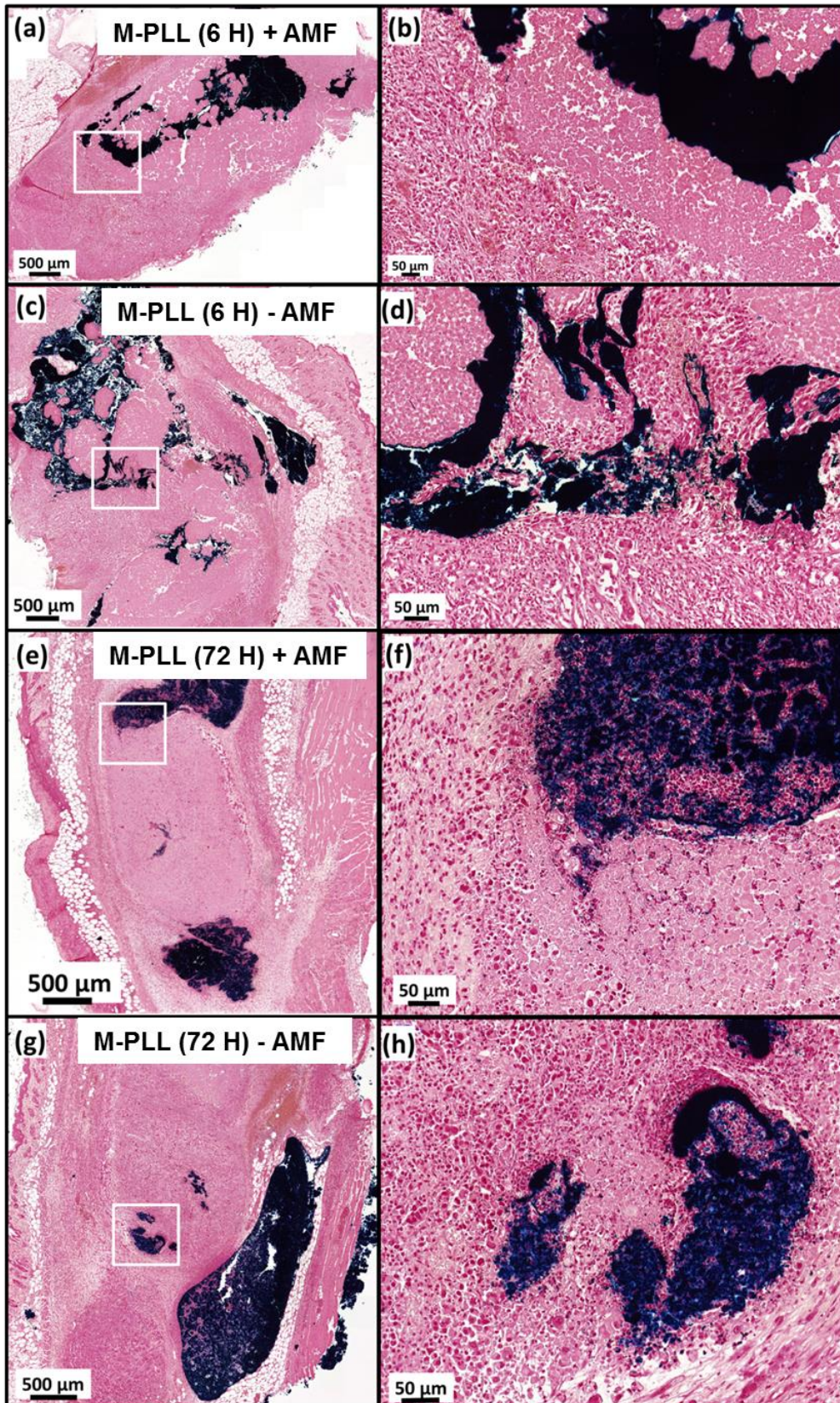


Figure S9

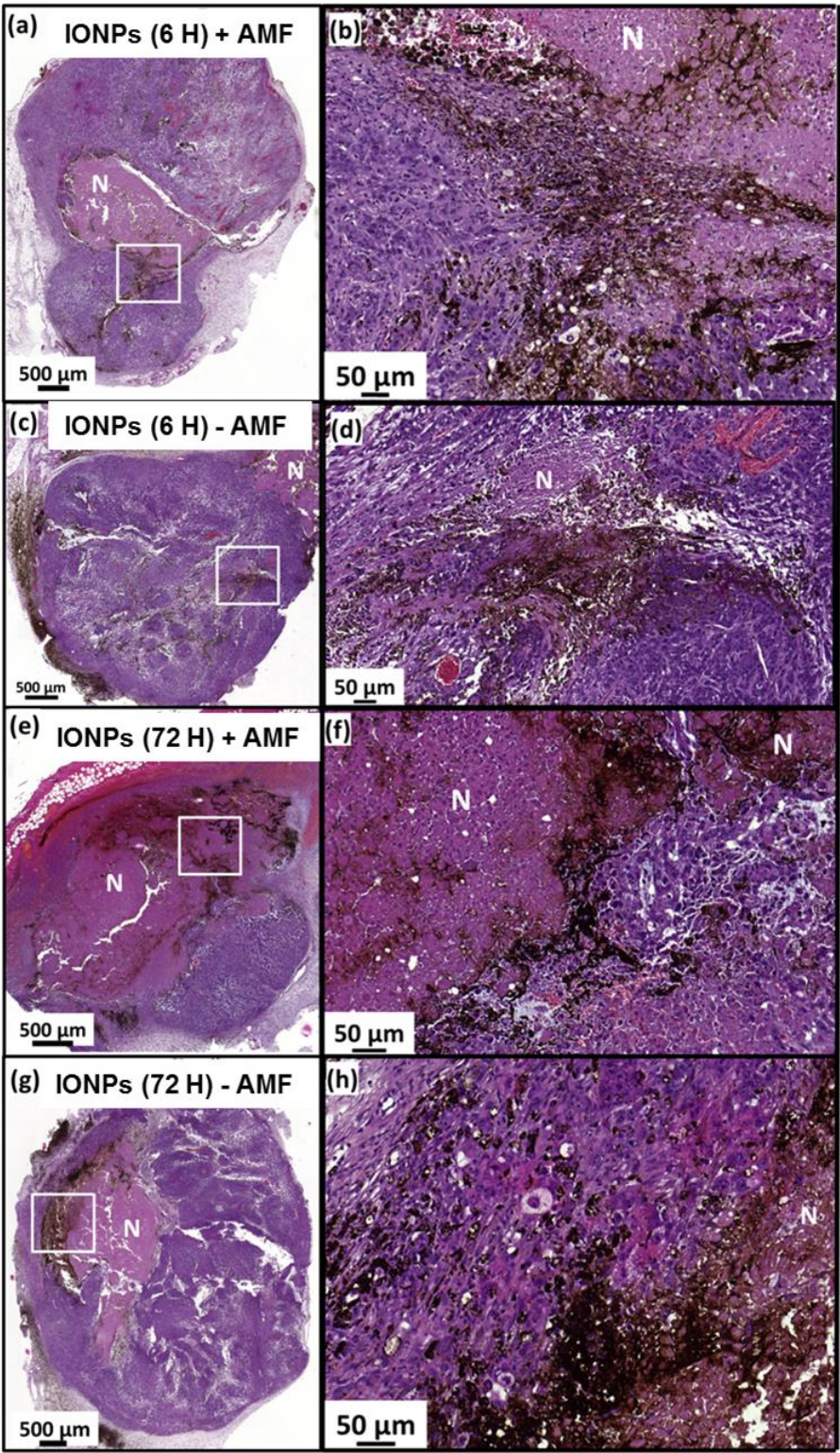


Figure S10

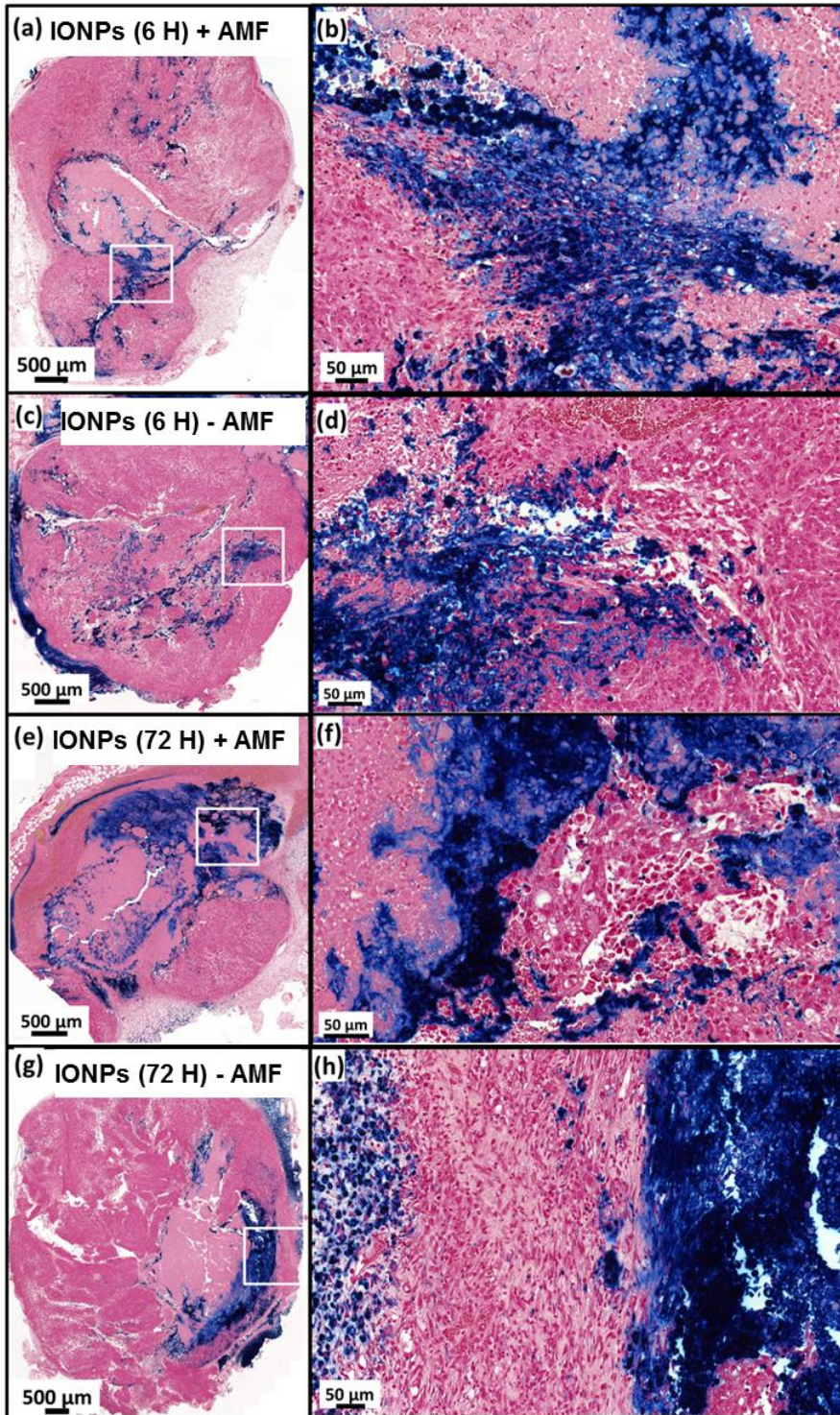


Figure S11

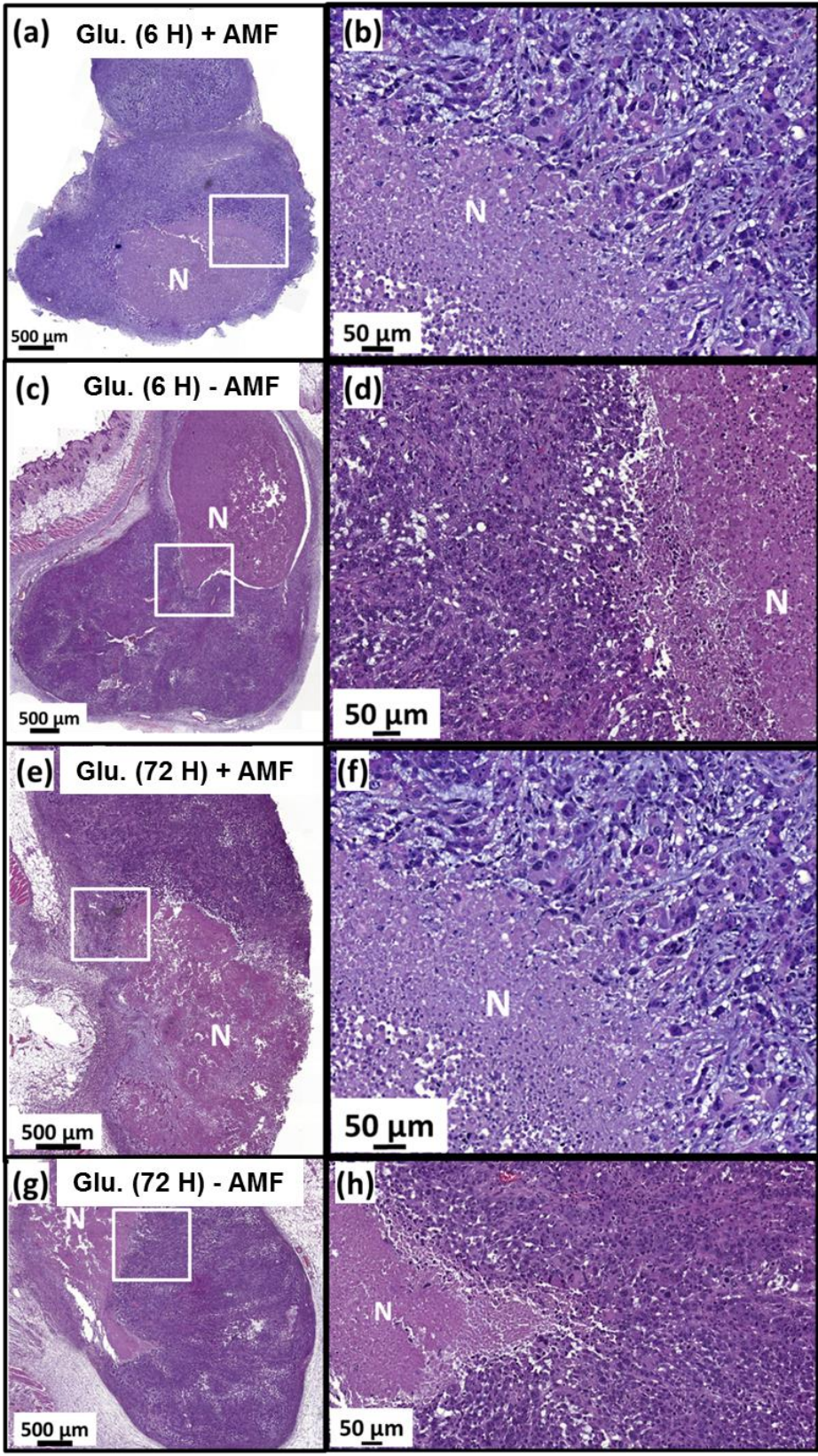


Figure S12

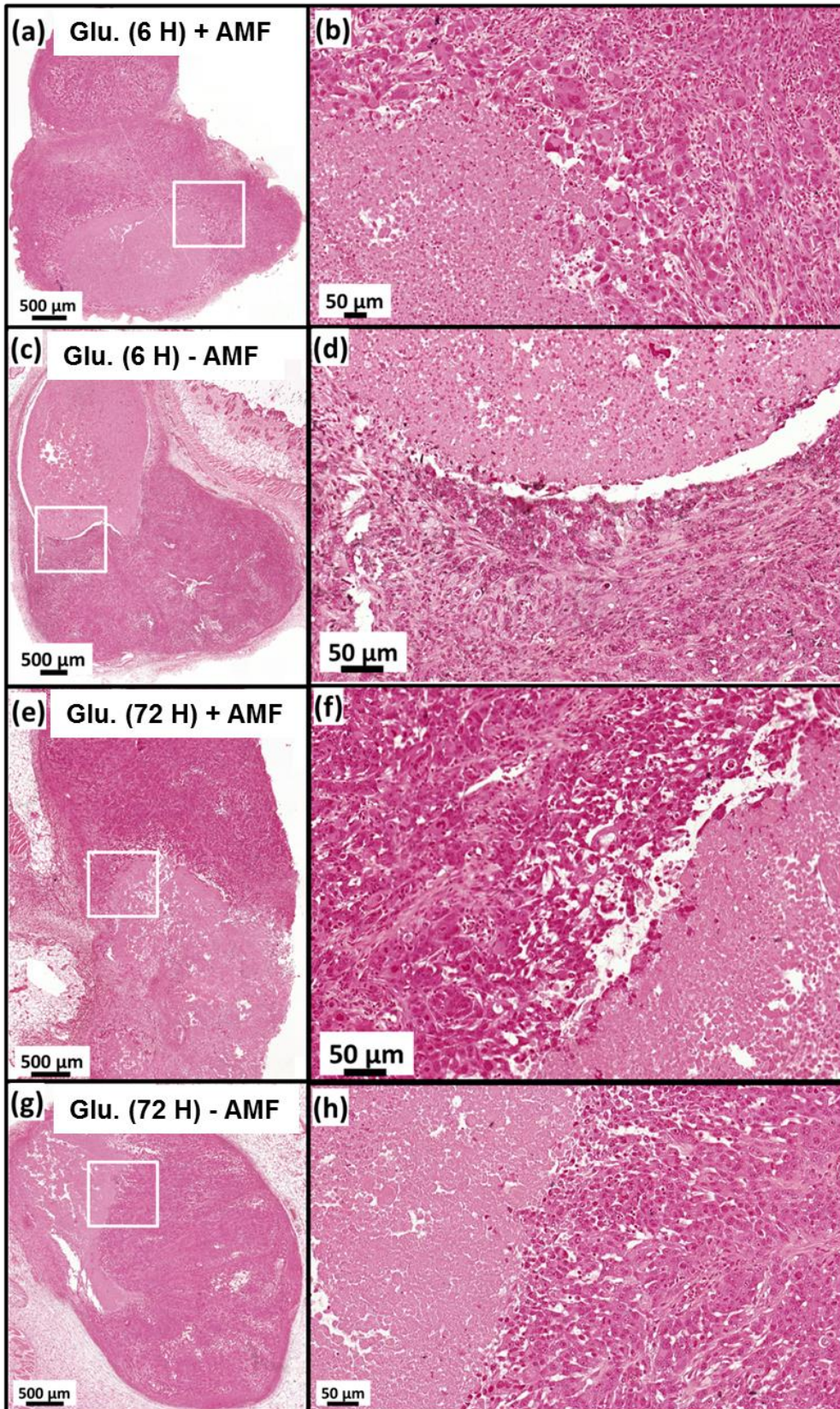


Figure S13